

Polarized electroweak bosons in W^+W^- production at the LHC including NLO QCD effects

Ansgar Denner and Giovanni Pelliccioli

Universität Würzburg, Institut für Theoretische Physik und Astrophysik, 97074 Würzburg, Germany

E-mail: ansgar.denner@physik.uni-wuerzburg.de,
giovanni.pelliccioli@physik.uni-wuerzburg.de

ABSTRACT: The measurement of polarization fractions of massive gauge bosons at the LHC provides an important check of the Standard Model and in particular of the Electroweak Symmetry Breaking mechanism. Owing to the unstable character of W and Z bosons, devising a theoretical definition for polarized signals is not straightforward and always subject to some ambiguity. Focusing on W -boson pair production at the LHC in the fully leptonic channel, we propose to compute polarized cross-sections and distributions based on the gauge-invariant doubly-resonant part of the amplitude. We include NLO QCD corrections to the leading quark-induced partonic process and also consider the loop-induced gluon-initiated process contributing to the same final state. We present results for both an inclusive setup and a realistic fiducial region, with special focus on variables that are suited for the discrimination of polarized cross-sections and on quantities that can be measured experimentally.

KEYWORDS: Electroweak bosons, Polarization, NLO QCD, Di-boson, LHC

Contents

1	Introduction	1
2	Details of the calculation	3
2.1	Definition of the polarized signals	3
2.2	Input parameters and selection cuts	7
3	Results	8
3.1	Inclusive phase-space region	10
3.2	Fiducial phase-space region	16
4	Conclusion	25

1 Introduction

The production of electroweak (EW) gauge bosons at the Large Hadron Collider (LHC) has been investigated intensively in recent years both theoretically and experimentally.

During Run 2 at 13 TeV centre-of-mass (CM) energy, the LHC accumulated enough luminosity to enable precise measurements of a large variety of multi-boson processes both in the light of probing the Standard Model (SM) of fundamental interactions and with the aim of hunting for new physics. The accumulated statistics allows for the measurement of observables that are difficult to extract from the data, like the polarizations of massive gauge bosons. Being unstable, W and Z bosons can only be produced off-shell and reconstructed from their hadronic or leptonic decay products. Therefore, the only way to get access to their polarization is to study their decay products, with a particular focus on the angular variables that have a direct dependence on the polarization mode of the decayed boson.

The analysis of polarization could serve as a probe of the SM gauge and Higgs sectors as well as a tool to discriminate between the SM and beyond-the-Standard-Model (BSM) theories. In particular, since the longitudinal polarization is a direct consequence of the Electroweak Symmetry Breaking (EWSB) mechanism, any deviation from the SM in the production of longitudinal weak bosons would provide valuable information.

A number of polarization measurements has been performed with LHC data at 8 TeV CM energy. The CMS and ATLAS collaborations have extracted polarization fractions and coefficients of angular distributions in W-boson production in association with jets [1, 2], in inclusive Z-boson production [3, 4], and in $t\bar{t}$ events [5, 6]. A combination of CMS and ATLAS W-boson polarization measurements in top-quark decays appeared very recently [7]. The first polarization measurement with 13 TeV data has been performed by ATLAS in $W^\pm Z$ production [8]. The increased luminosities expected in the high-luminosity

run of the LHC will enable polarization measurements even in processes with rather small cross-sections, like vector-boson scattering [9, 10].

Several theoretical results on polarized weak bosons at the LHC are available in the literature. A detailed study of W-boson polarization in W + jet production has been performed in Ref. [11] in the absence of lepton cuts. The effect of realistic selection cuts has been studied in Ref. [12] both in V + jets and in many other multi-boson production processes, including a few results at leading-order (LO) for WW and WZ production. The effect of selection cuts and their interplay with interferences between amplitudes for different polarizations has been investigated in Ref. [13]. The polarization of W and Z bosons in vector-boson scattering has been extensively studied in the fully leptonic channel at LO EW in Refs. [14, 15] using the PHANTOM Monte Carlo [16]. Recently, fiducial polarization observables have been analysed in fully leptonic $W^\pm Z$ production including next-to-leading (NLO) QCD and EW corrections both in a realistic LHC environment [17] and in an inclusive setup [18]. In particular, angular coefficients that can be extracted analytically from unpolarized distributions are directly related to the polarization fractions in the absence of lepton cuts. Extending this strategy in the presence of lepton cuts provides fiducial observables that, while being accessible at the LHC, can be very far from describing the polarization of decayed weak bosons. The calculation of polarized cross-sections has been automated in the MADGRAPH Monte Carlo [19], employing decay chains in the narrow-width approximation and including spin correlations via the MADSPIN package [20]. Very recently, the gluon-induced ZZ production with polarized bosons has been studied with the aim of enhancing the sensitivity to the $Zt\bar{t}$ coupling [21].

In this paper, focusing the discussion on the W^+W^- production at the LHC@13TeV, we propose a method to define signals with polarized weak bosons at the amplitude level, including also QCD radiative corrections. This actually represents an extension to NLO QCD of the method developed in vector-boson scattering with the PHANTOM Monte Carlo [14, 15]. The definition of polarized signals presented in this work relies on the double-pole approximation (DPA) [22–27], which is expected to be more accurate than the narrow-width approximation or a decay chain.

The production of W^+W^- pairs in the fully leptonic decay channel has been extensively studied at the theoretical level. Beyond its own importance as a clean signature at hadron colliders, it is an important irreducible background for Higgs searches, and provides a handle to probe the SM triple gauge-boson coupling. It has also been widely investigated in the context of direct BSM searches. The SM radiative corrections to the full process with leptonic decays are known up to next-to-next-to leading-order (NNLO) QCD and NLO EW [27–31]. All order resummation and parton-shower effects have also been studied [32–36]. NLO QCD results on polarized W^+W^- production within the SM and the Standard Model Effective Field Theory are shown in Ref. [37] for on-shell bosons W bosons.

However, a detailed phenomenological analysis of polarized W-boson pair production including off-shell effects is still missing in literature. The computation we present includes NLO QCD corrections to the leading $q\bar{q}$ partonic channel, and the LO predictions for the loop-induced gg partonic channel, which for the first time is studied in its polarization structure. Providing accurate SM predictions for polarized di-boson production is of great

importance both to further probe the SM itself and to investigate possible deviations from the SM triple gauge-boson couplings and other potential new-physics effects.

There is a long-standing experimental interest in the polarizations of W bosons in boson-pair production. They were investigated for example in electron-positron collisions at LEP [38] with the aim of probing anomalous gauge-boson couplings.

At the LHC, W -pair production has been measured by ATLAS [39, 40] with 13 TeV data, without the specific aim of extracting polarization fractions. Differently from $W^\pm Z$ and ZZ production, the presence of two neutrinos in the final state hampers the reconstruction of the two vector bosons, reducing the number of variables that discriminate among polarization states. However, the accumulated luminosity in Run 2 allows for the extraction of polarizations, *e.g.* by means of a multi-variate analysis of relevant observables based on SM Monte Carlo templates. Furthermore, the recent ATLAS results in $W^\pm Z$ production [8] and the foreseen measurements of polarizations in WW scattering with high-luminosity data [10] give us confidence that polarizations will soon be investigated in W -pair production.

This paper is organized as follows. In Sect. 2.1 we describe the strategy we use to define polarized cross-sections in W -pair production. In Sect. 2.2 we present the setup of our simulations, including SM parameters and selection cuts. Results for the production of one or two polarized bosons in an inclusive setup are shown in Sect. 3.1, while corresponding results in a realistic fiducial region are compiled in Sect. 3.2. We present both total cross-sections and differential distributions with a focus on the impact of QCD corrections on polarization fractions and, more in general, on polarized distributions for the relevant kinematic variables and observables. In Sect. 4 we draw our conclusions.

2 Details of the calculation

2.1 Definition of the polarized signals

A precise definition of polarized signals can be given only for on-shell particles. Since W and Z bosons are unstable particles, selecting their polarization states is always afflicted with some ambiguity. In this work, we define polarized cross-sections via an extension of the techniques used at LO in Refs. [14, 15] to NLO QCD. It is worth recalling the main steps taken to arrive at a well-behaved definition of polarized EW bosons at the amplitude level.

In all the following we focus on W -pair production, but everything is valid without modifications for any boson-pair production process in the fully leptonic decay channel, given that the two pairs of leptons have different flavours. Considering same flavour lepton pairs would require a more or less trivial extension of the DPA. The strategy can be directly transferred to define polarized cross sections for the production of arbitrary unstable particles.

The first obstacle towards the definition of polarized signals are the non-resonant contributions to the full process $pp \rightarrow e^+ \nu_e \mu^- \bar{\nu}_\mu + X$. Already at tree level in the SM (LO EW), di-boson production receives contributions from both resonant [Fig. 1(a)] and non-resonant diagrams [Fig. 1(b)]. The former diagrams give rise to an amplitude that can be factorized

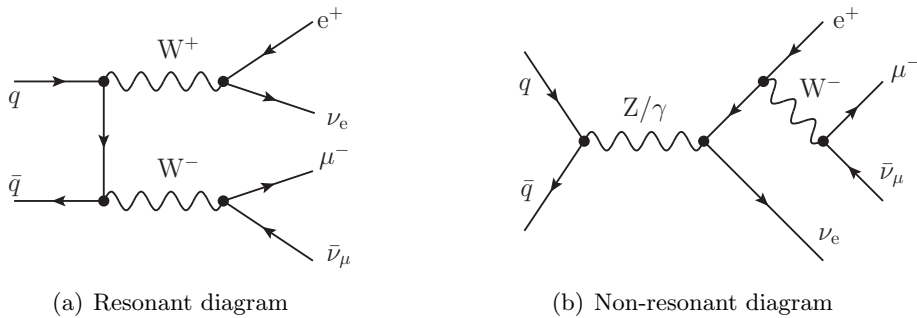


Figure 1. Sample tree-level diagrams for W^+W^- production at the LHC.

into production, propagation, and decay of vector bosons, *i.e.* they contain a contribution to vector-boson pair production. The latter diagrams do not involve two intermediate vector bosons, and a definition of corresponding polarizations does not make sense. In fact, non-doubly-resonant diagrams cannot be viewed as a contribution to vector-boson pair production, but should be treated as irreducible background and subtracted from the complete process. However, since non-resonant contributions are necessary to preserve gauge invariance, they cannot be dropped without further manipulating the resulting amplitude.

This issue is easily solved by using a narrow-width approximation, which however can be very inaccurate, since off-shell effects and spin correlations are completely neglected. Beyond simple decay-chain techniques, a better solution is provided by the MADSPIN method [19, 20] that preserves LO spin correlations and reintroduces an off-shell-ness of weak-boson propagators. Another approach, which has proven to be accurate in vector-boson scattering and other multi-boson signatures, is given by the DPA [22–27] or pole approximations in general [41, 42]: given a resonant amplitude, the numerator of the resonant diagrams is projected on shell to restore gauge invariance, while the Breit–Wigner modulation is kept with off-shell kinematics. This procedure can be viewed as a definition of the di-boson production contribution and provides a gauge-invariant separation of the complete process into W-pair production and the corresponding irreducible background. As the pole approximation, this separation does not only work for W-pair production but for arbitrary processes involving unstable particles. This technique has been employed to obtain the results presented in this paper.

Once W-pair production is properly isolated via the DPA in a gauge-invariant manner, individual polarized contributions can be defined. Note, however, that polarizations of massive states are not uniquely fixed. Let us consider a generic amplitude that involves the production of a W boson with momentum k (subamplitude \mathcal{P}_μ) and its decay into massless leptons with momenta l and $k - l$ (subamplitude \mathcal{D}_ν). In the 't Hooft–Feynman gauge such an amplitude reads

$$\mathcal{A}_{\text{res}} = \mathcal{P}_\mu(k) \frac{-g^{\mu\nu}}{k^2 - M_W^2 + i\Gamma_W M_W} \mathcal{D}_\nu(l, k - l). \quad (2.1)$$

Using polarization vectors ε_λ^μ for the W boson, the on-shell propagator numerator can be

rewritten as follows,

$$\begin{aligned}
\mathcal{A}_{\text{res}} &= \mathcal{P}_\mu(k) \frac{[\sum_{\lambda=L,\pm} \varepsilon_\lambda^{\mu*}(k) \varepsilon_\lambda^\nu(k)] - k^\mu k^\nu / M_W^2}{k^2 - M_W^2 + i\Gamma_W M_W} \mathcal{D}_\nu(l, k-l) \\
&= \sum_{\lambda=L,\pm} \frac{\mathcal{P}_\mu(k) \varepsilon_\lambda^{\mu*}(k) \varepsilon_\lambda^\nu(k) \mathcal{D}_\nu(l, k-l)}{k^2 - M_W^2 + i\Gamma_W M_W} - \frac{\mathcal{P}_\mu(k) k^\mu k^\nu \mathcal{D}_\nu(l, k-l)}{M_W^2 (k^2 - M_W^2 + i\Gamma_W M_W)} \\
&= \sum_{\lambda=L,\pm} \frac{\mathcal{M}_\lambda(k) \mathcal{M}_\lambda(l, k-l)}{k^2 - M_W^2 + i\Gamma_W M_W} + 0 =: \sum_{\lambda=L,\pm} \mathcal{A}_\lambda, \tag{2.2}
\end{aligned}$$

where the sum runs over the three physical polarizations, longitudinal ($\lambda = L$), left-handed ($\lambda = -$), and right-handed ($\lambda = +$). The term proportional to the boson momentum k vanishes upon contraction with the massless leptonic current \mathcal{D}_ν [second line of Eq. (2.2)]. Then, the numerator can be expressed as a sum over products of polarized matrix elements for the production $[\mathcal{M}_\lambda(k)]$ and the decay $[\mathcal{M}_\lambda(l, k-l)]$ of the polarized W bosons. Note also that would-be Goldstone-boson diagrams vanish thanks to the massless decay leptons. These simplifications hold within any R_ξ gauge. We stress that if the final leptons are massive, the additional term proportional to the boson momentum in Eq. (2.2) cancels against the would-be Goldstone-boson contributions, leaving the same sum over the physical polarization states.

It is worth noting that the polarization vectors introduced in Eq. (2.2) need to be defined in a specific reference frame. In all results presented in this paper, we choose the laboratory frame for this purpose. To be precise, for an on-shell vector boson with mass M , energy E , and momentum $p = \sqrt{E^2 - M^2}$ that propagates along the direction defined by the spherical angles θ_V and ϕ_V , the polarizations vectors read

$$\begin{aligned}
\varepsilon_-^\mu &= \frac{1}{\sqrt{2}}(0, \cos \theta_V \cos \phi_V + i \sin \phi_V, \cos \theta_V \sin \phi_V - i \cos \phi_V, -\sin \theta_V), \\
\varepsilon_+^\mu &= \frac{1}{\sqrt{2}}(0, -\cos \theta_V \cos \phi_V + i \sin \phi_V, -\cos \theta_V \sin \phi_V - i \cos \phi_V, \sin \theta_V), \\
\varepsilon_L^\mu &= \frac{1}{M}(p, E \sin \theta_V \cos \phi_V, E \sin \theta_V \sin \phi_V, E \cos \theta_V). \tag{2.3}
\end{aligned}$$

To obtain polarized cross-sections we need to square Eq. (2.2). The result is not simply the sum of squared polarized terms, since interferences among different polarization states arise,

$$|\mathcal{A}_{\text{res}}|^2 = \sum_\lambda |\mathcal{A}_\lambda|^2 + \sum_{\lambda \neq \lambda'} \mathcal{A}_\lambda^* \mathcal{A}_{\lambda'}. \tag{2.4}$$

Such interferences [the second term in Eq. (2.4)] are expected to vanish only for fully inclusive decays, *i.e.* in the absence of cuts on the decay leptons, but are non-zero otherwise [12–14]. However, interference effects play a non-negligible role even in an inclusive setup for W-pair production. From Eq. (2.4) it is evident that with a simple substitution in the propagator,

$$\sum_{\lambda'} \varepsilon_{\lambda'}^{\mu*} \varepsilon_{\lambda'}^\nu \longrightarrow \varepsilon_\lambda^{\mu*} \varepsilon_\lambda^\nu, \tag{2.5}$$

for a given polarization state λ ($= L, -, +$), we are able to compute polarized cross-sections with a Monte Carlo. The size of the interferences can then be easily deduced by comparing the unpolarized results [l.h.s. of Eq. (2.4)] with the sum of the polarized ones [first term on the r.h.s in Eq. (2.4)].

Since in W^+W^- production there are two vector bosons, not only singly-polarized but also doubly-polarized configurations can be investigated. To compute the doubly-polarized signals, we select a definite polarization state for both bosons, resulting in 9 different possible combinations. However, as usually done in experimental analyses, the left- and right-handed contributions of a single vector boson are combined by means of a coherent sum into the transverse one, which also includes the left–right interference term (which is non-zero in general). In the end we are left with four different combinations of longitudinal (L) and transverse (T) modes: $W_L^+W_L^-$, $W_L^+W_T^-$, $W_T^+W_L^-$, and $W_T^+W_T^-$. When computing singly-polarized signals, one boson has fixed polarization state (L or T), while the other one is kept unpolarized, *i.e.* we include the coherent sum of all of its polarization modes. In the following we consider singly-polarized results for the W^+ boson.

Finally, we include NLO QCD corrections. As detailed above, we use the DPA to define polarized cross-sections. In the literature, the DPA is usually applied only to contributions that feature Born-level kinematics, such as the LO or virtual corrections. In order to define polarized W bosons in all NLO contributions, we have to apply the DPA also to the real QCD corrections. Since we employ the Catani–Seymour scheme for the subtraction of infrared singularities [43], it has to be applied also to integrated and unintegrated subtraction dipoles, which turned out to be the most delicate part of the calculation.

The extension of this strategy to NLO EW is possible though slightly more complicated. Since both virtual and real corrections lead to non-factorizable but resonant contributions and real photons can be radiated off the resonant boson, various contributions have to be taken into account in the DPA. For each doubly-resonant term, polarized amplitudes have to be defined, and each term that is non-doubly-resonant has to be split off as background. This can be done following the line of reasoning in Refs. [24, 44, 45].

QCD radiative corrections only modify the production subprocess in di-boson production, leading to an easier implementation in a numerical code.

All results presented in this work have been obtained using RECOLA amplitudes [46, 47] and MOCANLO, which is a multi-channel Monte Carlo integration code that has already been used for several calculations at NLO QCD and EW accuracy [48–54]. For the purpose of this work, we have employed a private version of RECOLA that enables the separation of weak-boson polarizations in resonant SM amplitudes.

As a last comment of this section, we remark that the perturbative order which we consider in this work is not state-of-the-art, as we are neglecting both NNLO QCD and NLO EW corrections. However, the leading radiative corrections are represented by the NLO QCD ones, which are combined here with the results for the loop-induced gg partonic process. In general, the impact of NLO EW corrections is expected to be smaller than the one of QCD corrections. The results for $W^\pm Z$ production in Ref. [18] show that angular distributions and polarization observables are mildly modified by NLO EW corrections for what concerns the W boson in an inclusive setup. We therefore expect similar results in

W-pair production, at least in the absence of lepton cuts. However, we leave the treatment of NLO EW corrections to future work.

2.2 Input parameters and selection cuts

We investigate the process $pp \rightarrow e^+ \nu_e \mu^- \bar{\nu}_\mu + X$ for a proton–proton CM energy of 13 TeV assuming SM dynamics. At LO, this process receives contributions from $q\bar{q}$ initial states only. The LO [$\mathcal{O}(\alpha^4)$] and NLO QCD [$\mathcal{O}(\alpha_s \alpha^4)$] predictions are computed in the five-flavour scheme. We choose the following on-shell EW vector-boson masses and widths [55],

$$\begin{aligned} M_W^{\text{OS}} &= 80.3790 \text{ GeV}, & \Gamma_W^{\text{OS}} &= 2.0850 \text{ GeV}, \\ M_Z^{\text{OS}} &= 91.1876 \text{ GeV}, & \Gamma_Z^{\text{OS}} &= 2.4952 \text{ GeV}, \end{aligned} \quad (2.6)$$

which are converted into the corresponding pole values by means of [56],

$$M_V = \frac{M_V^{\text{OS}}}{\sqrt{1 + (\Gamma_V^{\text{OS}}/M_V^{\text{OS}})^2}}, \quad \Gamma_V = \frac{\Gamma_V^{\text{OS}}}{\sqrt{1 + (\Gamma_V^{\text{OS}}/M_V^{\text{OS}})^2}}. \quad (2.7)$$

Further SM parameters are chosen as

$$\begin{aligned} M_H &= 125 \text{ GeV}, & \Gamma_H &= 0.00407 \text{ GeV}, \\ m_t &= 173 \text{ GeV}, & \Gamma_t &= 0 \text{ GeV}, \\ G_\mu &= 1.16638 \cdot 10^{-5} \text{ GeV}^{-2}. \end{aligned} \quad (2.8)$$

While the Higgs and top parameters are irrelevant for the quark-induced processes, they enter the calculation of the gluon-induced channel. We consider massless bottom quarks. Even if we work in the five-flavour scheme, the $b\bar{b}$ -initiated partonic channel is neglected, since it is strongly PDF suppressed with respect to other quark flavours. The parton distribution functions (PDF) are passed to MOCANLO via the LHAPDF6 interface [57]. We use NNPDF3.1 PDFs [58] computed with $\alpha_s(M_Z) = 0.118$ [NNPDF31.(n)lo_as_0118 for (N)LO]. The G_μ scheme is employed for fixing the EW coupling, and the weak vector bosons are treated in the complex-mass scheme [25, 59, 60].

We also present results for the loop-induced gluon-initiated partonic processes $gg \rightarrow e^+ \nu_e \mu^- \bar{\nu}_\mu$. For this, we employ the same parameters described above, apart from the b-quark mass which is now set to $M_b = 4.7 \text{ GeV}$. However, we keep working in the five-flavour scheme. We use the same PDF choice as for NLO QCD corrections to the quark-induced process.

In all computations the factorization and renormalization scales are set to the W pole mass, $\mu_F = \mu_R = M_W$.

We consider two different sets of selection cuts. To validate the polarized distributions we use a first setup (labelled *inclusive*) that only involves a technical cut on the charged-lepton transverse momentum, $p_T^\ell > 0.01 \text{ GeV}$, whose effects on the results are completely negligible, and a jet veto on additional jets with $p_{T,j} > 35 \text{ GeV}$, $|\eta_j| < 4.5$. We then consider a second setup (labelled *fiducial*) that mimics the fiducial signal region defined in a recent ATLAS measurement [40]:

- minimum transverse momentum of the charged leptons, $p_{T,\ell} > 27$ GeV;
- maximum rapidity of the charged leptons, $|\eta_\ell| < 2.5$;
- minimum missing transverse momentum, $p_{T,\text{miss}} > 20$ GeV;
- the same jet veto (no jets with $p_{T,j} > 35$ GeV, $|\eta_j| < 4.5$) as in the inclusive setup;
- minimum invariant mass of the charged lepton-pair system, $M_{e^+\mu^-} > 55$ GeV.

The last invariant-mass cut is applied to reduce the Higgs background down to approximately 1% of the total WW-production cross-section. This is important mostly in the study of the gluon-induced partonic process, for which in any case we exclude the Higgs peak region by imposing $M_{2\ell 2\nu} > 130$ GeV. Note that in the ATLAS paper [40] a transverse momentum cut ($p_{T,e^+\mu^-} > 30$ GeV) is also applied to the charged lepton pair to suppress the Drell–Yan background. However, we do not use this cut in the following, since it is motivated by experimental mis-reconstruction of the final state. The top-production background is suppressed in the ATLAS analysis by means of a b-jet veto (no b jets with $p_{T,b} > 20$ GeV and $|\eta_b| < 2.5$). In our discussion we assume a perfect b-jet veto for simplicity.

3 Results

In this section, we present phenomenological results for polarized signals in W-pair production. We have investigated both singly-polarized and doubly-polarized configurations, since the experimental interest lies both in the single-boson polarization fractions and in the extraction of the doubly-longitudinal cross-section. Naïvely one could expect that the doubly-polarized cross-sections are directly related to the singly-polarized ones. This statement is wrong, as the two W-boson spin states are strongly correlated in di-boson kinematics. This is due to the absence of additional jets in the final state and to the constrained angular momentum balance of the initial state that features two spin-1/2 particles in the leading partonic channel. Such a correlation is weaker if the weak-boson pair is produced with additional jets [14]. However, even in that case the zero-correlation hypothesis is definitely not realistic.

In the following, we also evaluate the contributions of the non-resonant irreducible background and effects of interferences among polarizations at the level of total and differential cross-sections. The non-resonant background is defined as the difference between results based on full matrix elements (full, for simplicity) and the unpolarized results computed with the DPA as described in Sect. 2.1. Their size is *a priori* expected to be of the order of the intrinsic error of the DPA [$\mathcal{O}(\alpha)$].

Interferences among different polarization states are estimated as the difference between the unpolarized DPA results and the sum of polarized DPA ones [see Eq. (2.4)]. Such a sum runs over two singly-polarized contributions, *i.e.* T and L, or four doubly-polarized ones, *i.e.* TT, TL, LT, LL states: in the former case, interferences are expected

to be slightly smaller than in the latter one, as the interferences corresponding to the unpolarized bosons are implicitly included in the calculation. Even if, in general, interferences are expected to vanish in the absence of lepton cuts, there can be non-trivial effects due to the correlations of the polarizations of the two produced bosons in the doubly-polarized case and in distributions in the singly-polarized case.

We are going to present results at LO and NLO QCD for the leading $q\bar{q}$ channel and combine them with LO results for the gg channel.

The loop-induced production of W^+W^- pairs with two initial-state gluons gives a contribution at $\mathcal{O}(\alpha_s^2\alpha^4)$. Although it is formally part of the NNLO QCD corrections to W -pair production, it is enhanced by the gluon luminosity in the proton. It can be computed independently as it only involves ultraviolet- and infrared-finite amplitudes. We note that for massless quarks and leptons only doubly- W -resonant diagrams contribute to the gluon-induced process [61]. Among them, only box diagrams and one triangle Higgs-exchange diagram are non-vanishing. The triangle diagram, proportional to the top-quark Yukawa coupling, is negligible if the Higgs-mass region is cut away. As a consequence, the DPA reproduces the full result much better than in the quark-induced channels.

For the gg channel, we exclude the Higgs-resonance peak by an invariant-mass cut $M_{2\ell 2\nu} > 130 \text{ GeV}$. This reduces the cross-section for $gg \rightarrow e^+\nu_e\mu^-\bar{\nu}_\mu$ by 5% relative to the one computed from the complete invariant-mass spectrum. Given that the gluon-induced contribution is roughly 7% of the NLO QCD total cross-section for $q\bar{q}$, the Higgs signal accounts for a few permille in the combined cross-section.

Before presenting results, we remind the reader that we consider a jet veto (no jets in the region $p_{T,j} > 35 \text{ GeV}$, $|\eta_j| < 4.5$). This selection is applied in W^+W^- production to suppress large contributions from additional QCD radiation. If such a veto is not required, the results (both polarized and unpolarized) change noticeably, as the additional jet recoils against the W^+W^- system. In particular, avoiding the jet veto leads to a substantial improvement of the quality of the DPA at NLO QCD, as doubly-resonant diagrams contribute also in regions where they would be excluded (*e.g.* large missing transverse momentum) if the jet veto was applied. Nonetheless, dropping the jet veto would mean that W^+W^-j production (LO accurate) is not suppressed anymore with respect to W^+W^- production. Therefore the polarized predictions would not pertain exactly to di-boson production. In all the following we understand the jet veto described in Sect. 2.2 to be applied.

A further comment should be made on the jet veto. The results we are going to show concern fixed-order predictions in perturbative QCD. It is well known [62, 63] that applying a jet-veto in di-boson production leads to an enhancement of higher-order corrections due to large logarithms stemming from the ratio between the di-boson invariant mass ($\gtrsim 2M_W$) and the jet-veto scale. While this affects total cross-sections and shapes of distributions, we do not expect that the resummation of jet-veto logarithms would sizeably affect the polarization fractions. This is supported by the fact that polarization fractions exhibit a very mild dependence on the QCD scale, as shown below. Moreover, for di-boson production with leptonic decays, the QCD corrections are related only to the initial state, while the polarization dependence is tied to the final state.

	LO	NLO QCD	K -factor	Δ_{gg}
full	871.4(4) ^{+4.2%} _{-5.1%}	932.0(9) ^{+1.8%} _{-2.3%}	1.07	1.05
unpolarized (DPA)	859.1(2) ^{+4.2%} _{-5.1%}	920.7(5) ^{+1.9%} _{-2.4%}	1.07	1.05
$W_L^+ W_{\text{unpol}}^-$ (DPA)	224.0(1) ^{+5.0%} _{-6.3%}	249.2(2) ^{+2.0%} _{-2.5%}	1.11	1.03
$W_T^+ W_{\text{unpol}}^-$ (DPA)	635.0(1) ^{+4.0%} _{-4.8%}	671.4(4) ^{+1.8%} _{-2.2%}	1.06	1.06
$W_L^+ W_L^-$ (DPA)	16.22(1) ^{+5.2%} _{-6.0%}	25.19(2) ^{+2.4%} _{-3.3%}	1.55	1.08
$W_L^+ W_T^-$ (DPA)	207.8(1) ^{+5.0%} _{-6.0%}	224.0(1) ^{+2.0%} _{-2.6%}	1.08	1.03
$W_T^+ W_L^-$ (DPA)	253.9(1) ^{+4.8%} _{-5.8%}	266.3(2) ^{+2.0%} _{-2.5%}	1.05	1.02
$W_T^+ W_T^-$ (DPA)	381.1(1) ^{+3.3%} _{-4.1%}	404.9(2) ^{+1.6%} _{-2.0%}	1.06	1.08

Table 1. Total cross-sections (in fb) in the inclusive setup for the unpolarized, singly-polarized and doubly-polarized W^+W^- production at the LHC. Uncertainties are computed with 7-point scale variations. K -factors are computed as ratios of NLO QCD over LO integrated cross-sections. The contribution of the gluon-induced channel is shown relative to the NLO QCD results for $q\bar{q}$.

3.1 Inclusive phase-space region

In this section we present results obtained in the inclusive setup. For W -pair production, the final state only involves the decay products of the two W bosons, which are produced almost back-to-back, up to an additional jet with small p_T at NLO. Therefore, the kinematic variables of decay products are more strongly correlated than in other multi-boson signatures, such as in vector-boson scattering. This affects the polarized signals leading to interesting results that could be naïvely considered as unexpected.

In Table 1 we show the total cross-sections (in fb) for all relevant polarizations, including both singly- and doubly-polarized results. The numerical errors on the central values are indicated in parentheses. The percentage scale uncertainties, extracted with 7-point variations around the central scale, are provided in superscripts and subscripts. Note that the DPA cross-sections are identically zero for $M_{2\ell 2\nu} < 2M_W$ by definition. The contribution to the full cross-section of the region below $2M_W$ is merely 1.3%. As a general comment, the transverse polarization strongly dominates over the longitudinal one, as in most multi-boson production processes [11, 12]. This implies that K -factor, scale variations, and enhancement due to the gg channel for transverse W bosons are very similar to the unpolarized case. Results with at least one longitudinal boson show slightly larger K -factors compared to the transverse ones: 1.11 for the singly-longitudinal (dominated by the transverse component of the unpolarized boson), 1.55 for the LL, despite the application of the jet veto. After combining with the gluon-induced channel, the unpolarized cross-section is enhanced by 5%, the LL and TT cross-sections by 8%, and the mixed ones by just 2–3%. The difference between the two mixed doubly-polarized cross-sections results from the different angular momentum balance in the u-type and d-type quark-initiated partonic channels. Since no cuts are imposed on the leptons, the sum of singly- or doubly-polarized

cross-sections is identical to the unpolarized DPA cross-section within integration errors. This is further confirmed by the analysis of differential distributions.

As a validation of our definition of polarized vector bosons, we consider the distributions in the decay angles of leptons θ_ℓ^* and ϕ_ℓ^* computed in the corresponding W-boson rest frame. The differential distributions in these variables directly reflect the polarization modes of the decayed vector boson. An ambiguity is related to the reference axis with respect to which the leptonic angular variables θ_ℓ^* , and ϕ_ℓ^* in the weak-boson rest frame are defined.

Using the so-called helicity coordinate system [11], we choose as reference axis the direction of the W boson in the laboratory frame. With this choice, the polarization vectors in the laboratory frame and the helicity frame are directly related by a boost along the reference axis, and the dependence on θ_ℓ^* and ϕ_ℓ^* directly reflects the polarizations in the laboratory frame. This would not be the case if the reference axis was chosen as the direction of the W boson in the CMS frame of the W-boson pair.

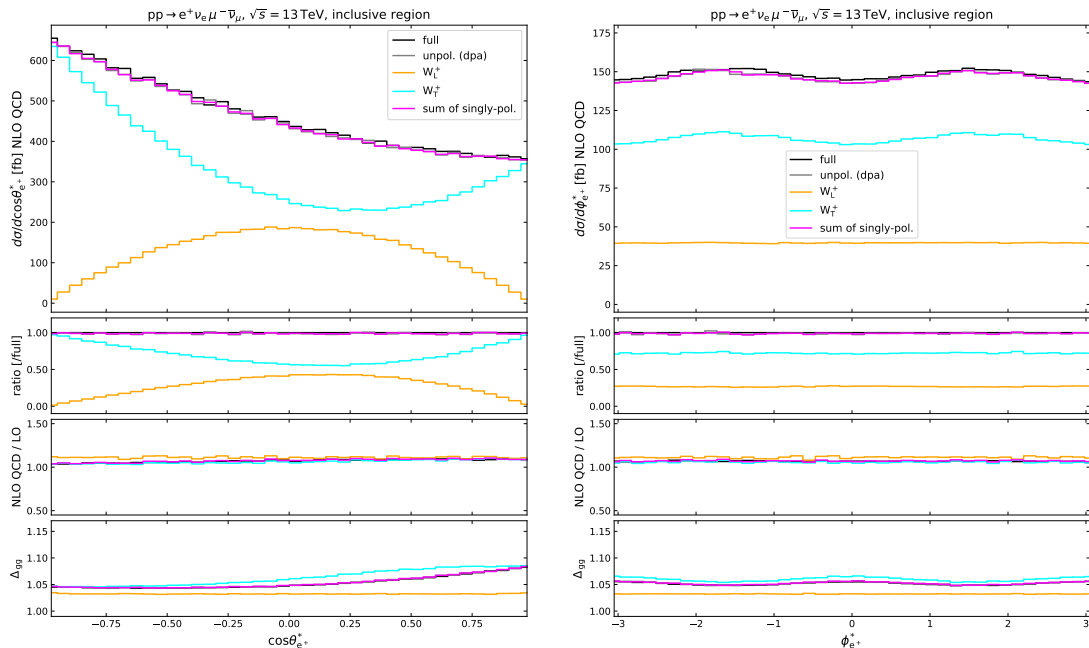
We consider singly-polarized distributions for the W^+ boson decaying to $e^+\nu_e$, but analogous results can be obtained for the W^- boson. We stress that, while being sensitive to the polarization state of the weak bosons, these angular variables require the full reconstruction of both W bosons separately, which is impossible with two neutrinos in the final state. However, they are relevant to validate the definition of polarized cross-sections in Monte Carlo simulations. In the corresponding differential distributions, shown in Fig. 2, we observe that the interferences are compatible with zero in the inclusive setup, as expected. The K -factor is practically constant for both the polarized and the unpolarized configurations.

The most important reason to study distributions in θ_e^* and ϕ_e^* lies in the possibility of extracting analytically the polarization fractions from the unpolarized distribution. At LO in the EW coupling, the differential cross-section for the production of an unpolarized W^+ boson reads

$$\begin{aligned} \frac{d\sigma}{d\cos\theta_e^* d\phi_e^* dX} &= \frac{d\sigma}{dX} \frac{3}{16\pi} \left[(1 + \cos^2\theta_e^*) + (A_0/2)(1 - 3\cos^2\theta_e^*) + A_1 \sin 2\theta_e^* \cos\phi_e^* \right. \\ &\quad + (A_2/2) \sin^2\theta_e^* \cos 2\phi_e^* + A_3 \sin\theta_e^* \cos\phi_e^* + A_4 \cos\theta_e^* \\ &\quad \left. + A_5 \sin^2\theta_e^* \sin 2\phi_e^* + A_6 \sin 2\theta_e^* \sin\phi_e^* + A_7 \sin\theta_e^* \sin\phi_e^* \right], \end{aligned} \quad (3.1)$$

where X is a generic (set of) kinematic variable(s), independent of θ_e^* and ϕ_e^* . The coefficients A_i represent scalar quantities that are related to the polarization of the produced W boson, and depend on the variable X . If the full ϕ_e^* range is accessible, which is the case if no cuts are imposed on the positron and the related neutrino, the interferences vanish upon integrating out the azimuthal angle leaving a simple functional dependence on θ_e^* :

$$\begin{aligned} \frac{d\sigma}{d\cos\theta_e^* dX} &= \frac{d\sigma}{dX} \frac{3}{8} \left[(1 + \cos^2\theta_e^*) + (A_0/2)(1 - 3\cos^2\theta_e^*) + A_4 \cos\theta_e^* \right] \\ &= \frac{d\sigma}{dX} \frac{3}{8} \left[2f_L \sin^2\theta_e^* + f_-(1 - \cos\theta_e^*)^2 + f_+(1 + \cos\theta_e^*)^2 \right], \end{aligned} \quad (3.2)$$



(a) Cosine of theta angle of e^+ in the W^+ CM frame. (b) Azimuthal angle of e^+ in the W^+ CM frame.

Figure 2. Distributions in the positron angular variables $\cos\theta_e^*$ and ϕ_e^* defined in the W^+ rest frame in the inclusive region. Singly-polarized and unpolarized results are shown. From top down: NLO QCD differential cross-sections for the $q\bar{q}$ channel, ratios over the full (unpolarized), K -factors (NLO QCD/ LO), and enhancement of the NLO QCD cross-sections due to the gg channel.

where the polarization fractions f_i are related to A_i by simple linear combinations, and are such that $f_L + f_+ + f_- = 1$. This expression can be used to extract polarization fractions for processes which are dominated by vector-boson resonances, like W -pair production, provided that the decay products can be uniquely identified.

We have extracted the polarization fractions from the unpolarized DPA distribution in $\cos\theta_e^*$ by means of suitable projections on (3.2) in the same fashion as in Ref. [14] and combined them into f_L and $f_T = f_+ + f_-$. These are compared with polarization fractions that are obtained as ratios of the polarized cross-sections (computed with the Monte Carlo) over the unpolarized DPA one. The agreement is almost perfect, as can be seen in Table 2. Note that the results extracted from unpolarized angular distributions (analytic) agree perfectly with Monte Carlo predictions not only at the normalization level (total cross-sections) but also for the shapes of singly-polarized distributions in $\cos\theta_e^*$. The LO longitudinal polarization fraction experiences a 1% enhancement due to NLO corrections, which is balanced by a corresponding decrease in the transverse fraction. We also observe that the obtained polarization fractions are very stable against scale variations both at LO and NLO QCD. The polarization fractions presented in Table 2 concern the complete inclusive phase-space region, but a very good agreement ($< 1\%$) is found even in specific ranges of the W^+ transverse momentum and rapidity.

As can be deduced from the asymmetry of the distribution for transverse W^+ boson in

	LO		NLO QCD	
non-resonant backgr. interferences	0.0142(5) $^{+0.0002}_{-0.0003}$ < 10 ⁻⁴		0.0111(9) $^{+0.0003}_{-0.0003}$ < 10 ⁻⁴	
	MC	analytic	MC	analytic
W _L ⁺ W _{unpol} ⁻ (DPA)	0.261(1) $^{+0.002}_{-0.002}$	0.260(3) $^{+0.002}_{-0.003}$	0.271(1) $^{+0.001}_{-0.001}$	0.272(3) $^{+0.001}_{-0.001}$
W _T ⁺ W _{unpol} ⁻ (DPA)	0.739(3) $^{+0.003}_{-0.002}$	0.740(5) $^{+0.002}_{-0.002}$	0.729(3) $^{+0.002}_{-0.001}$	0.728(6) $^{+0.001}_{-0.001}$

Table 2. Fractions for a polarized W⁺ boson produced in association with an unpolarized W⁻ boson in the inclusive setup. Uncertainties are computed with 7-point scale variations. The polarization fractions from Monte Carlo (**MC**) are obtained by taking the ratio of polarized total cross-sections over the unpolarized one in the DPA. The same holds for contributions of the non-resonant irreducible background and interferences. The **analytic** polarization fractions are obtained by suitable projections of the unpolarized DPA cross-section.

Fig. 2(a) combined with Eq. (3.2), the left-handed polarization is almost twice the right-handed one in the $q\bar{q}$ channel ($f_+/f_- \approx 0.52$), in good agreement with the corresponding result of Table 2 in Ref. [12]. This asymmetry is due to the fact that the process is $q\bar{q}$ initiated, so that the W bosons are preferably generated with left-handed helicity. As the produced bosons have preferably small p_T , angular-momentum arguments [11] imply that the W⁺ boson originating from $u\bar{u}/c\bar{c}$ annihilation is mostly left handed ($f_- \approx 0.67$, $f_+ \approx 0.11$), while in $d\bar{d}/s\bar{s}$ it is mostly right handed ($f_- \approx 0.21$, $f_+ \approx 0.47$). Weighting the polarization fractions with the relative PDF factors between the two quark–antiquark channels, one recovers $f_+/f_- \approx 0.52$. On the contrary, the loop-induced channel gives perfect left–right symmetric distributions for transverse W⁺ bosons, as expected for zero-charge, spin-1 massless particles in the initial state.

As seen in Fig. 2(b), the ϕ_e^* distribution for the longitudinal polarization is flat, as expected from the decay amplitudes, while the transverse one receives a $\cos 2\phi_e^*$ modulation, as the interference between the left- and right-handed modes gives non-vanishing ϕ_e^* -dependent terms. This is exactly the origin of the ϕ_e^* dependence in Eq. (3.1). We have checked that simulating the production of left-handed or right-handed W bosons separately gives flat distributions, as the ϕ_e^* dependence disappears in the squared amplitudes ($\mathcal{A}_\pm \propto e^{\pm i\phi_e^*}$). Note that this argument is no longer true in the presence of lepton cuts. An interesting aspect is that in the gluon-induced process the spin-1 nature of the incoming partons also gives a $\cos 2\phi_e^*$ modulation but with opposite sign with respect to the quark-induced channel.

So far, we have provided a number of arguments that prove the quality of polarization separation at the amplitude level and in the Monte Carlo simulation. This has been validated not only for singly-polarized signals but also for the doubly-polarized ones. Considering the $\cos \theta_\mu^*$ distribution for a longitudinal W⁺ and an unpolarized W⁻ boson, we have extracted via suitable projections [14] the doubly-polarized distributions (LL, LT) and found them to agree perfectly with the results directly simulated with the Monte

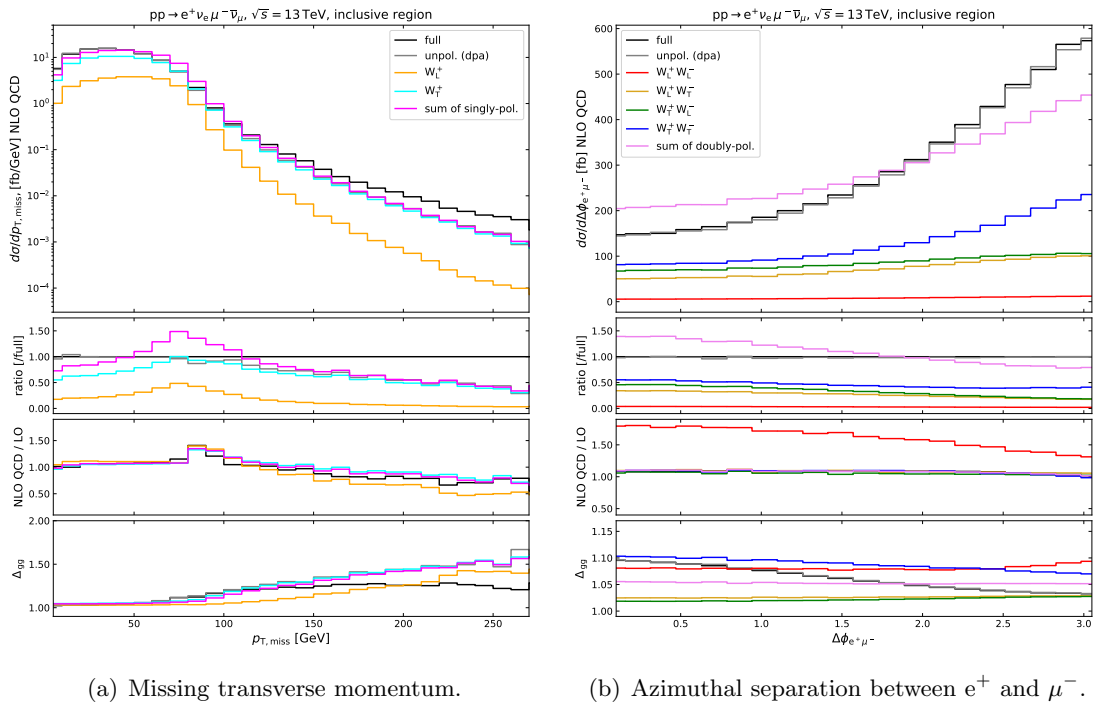


Figure 3. Distributions in the missing transverse momentum and in the azimuthal separation between the two charged leptons in the inclusive region. Singly-polarized results are shown in Fig. 3(a), doubly-polarized ones in Fig. 3(b). Same subplot structure as in Fig. 2.

Carlo. Analogously, we have extracted the TL and TT components from the transverse-unpolarized $\cos\theta_\mu^*$ distributions. These checks further confirm that the proposed definition of polarized signals is very well behaved.

Furthermore, the integrated cross-sections and the distributions in $\cos\theta_e^*$ presented so far confirm that the interferences among polarization modes vanish upon integration over the azimuthal decay angles in the absence of lepton cuts. This holds for most of the kinematic observables that can be reconstructed at the LHC.

However, for some observables, even in the inclusive setup, the polarization separation does not provide predictions that can easily be interpreted as polarized predictions. A first example is given by the distribution in the missing transverse momentum, shown for the polarized and unpolarized cases in Fig. 3(a). It is well known that in kinematic regions that are not dominated by doubly-resonant diagrams the DPA describes the full computation badly. This is the case for the region of large missing transverse momentum, where the doubly-resonant contributions are suppressed and the singly-resonant diagrams (dropped in the DPA) give a relevant contribution to the full calculation already at Born level [27]. This translates into a suppression of polarized distributions, as can be seen for all DPA curves in Fig. 3(a) for $p_{T,\text{miss}} > 100$ GeV. The discrepancy between the unpolarized DPA and full results reaches -50% already at moderate values $p_{T,\text{miss}} \approx 200$ GeV.

Furthermore, even in the region where the DPA behaves well ($p_{T,\text{miss}} \lesssim 100$ GeV),

the sum of singly-polarized distributions does not reproduce the unpolarized DPA one, pointing out large interferences between the transverse and longitudinal modes. In fact, selecting the missing transverse momentum in a certain range imposes restrictions on the lepton kinematics, specifically on a variable that is not directly related to a single W boson, and impedes the cancellation of interferences. A similar situation is observed also for the distributions in the transverse momentum of the positron–muon pairs. This effect has been found also in W^+W^- scattering [14].

The above comments apply to both LO and NLO QCD results. The K -factor is similar for the various polarized and unpolarized distributions: only the longitudinal polarization features a somewhat smaller K -factor in the large $p_{T,\text{miss}}$ regime. In the gluon-induced channel, the doubly-resonant diagrams are dominant even at large $p_{T,\text{miss}}$, leading to a better description of the full matrix elements and a better modelling of the polarized signals.

Another interesting variable that discloses some surprises in the inclusive setup is the azimuthal separation between the two charged leptons shown in Fig. 3(b). In this case the unpolarized DPA distribution describes the full result (with at most 2% deviation) very well. However, the sum of doubly-polarized signals is far from the unpolarized one, *i.e.* large interferences characterize this observable. They amount to +40% for $\Delta\phi_{e^+\mu^-} \approx 0$ and –30% for $\Delta\phi_{e^+\mu^-} \approx \pi$. The same happens for singly-polarized distributions. Note that such an effect can only result from interferences between the longitudinal and the transverse mode, as the left–right interference is already accounted for in the definition of the cross-sections for transverse polarization. A similar situation has been found in the W^+W^- decay of a Higgs boson produced in gluon fusion [64], while it is absent in vector-boson scattering [14]. Whereas in vector-boson scattering the two W bosons are produced mostly in the central region, in di-boson production they feature back-to-back kinematics inducing correlations between the decay angles of the two charged leptons. This is supported by the fact that this large effect is partially reduced upon omitting the jet veto in NLO QCD corrections. Since such interferences are not found for ZZ production, as we checked numerically, they are apparently enhanced in the back-to-back kinematics by the purely left-handed nature of the W-boson coupling to leptons.

In the gluon-induced channel the interferences show an opposite behaviour, being positive for $\Delta\phi_{e^+\mu^-} \approx \pi$ and negative close to 0. However, the combination of all partonic processes features the same behaviour as the dominant quark-induced process.

It is evident that the correlation between the polarizations of the two W bosons affects the polarized cross-sections in W^+W^- production much more than in the presence of additional jets, such as in W^+W^-jj production. As a consequence, interferences can appear even in the absence of cuts on single leptons, reducing the number of variables that allow for an interpretation of unpolarized distributions as a sum of the polarized ones. Nevertheless, the results of this section already show that defining accurately polarized signals and accounting for interferences is definitely needed to enable the correct extraction of polarized information from LHC data.

	LO	NLO QCD	K -factor	Δ_{gg}
full	202.02(3) ^{+4.6%} _{-5.5%}	220.16(8) ^{+1.8%} _{-2.2%}	1.09	1.06
unpolarized (DPA)	195.91(3) ^{+4.7%} _{-5.5%}	214.48(9) ^{+1.8%} _{-2.2%}	1.09	1.06
$W_L^+ W_{\text{unpol}}^-$ (DPA)	50.94(1) ^{+5.5%} _{-6.5%}	57.42(4) ^{+1.9%} _{-2.6%}	1.13	1.04
$W_T^+ W_{\text{unpol}}^-$ (DPA)	141.72(2) ^{+4.3%} _{-5.1%}	152.84(9) ^{+1.7%} _{-2.1%}	1.08	1.07
$W_L^+ W_L^-$ (DPA)	6.653(1) ^{+4.9%} _{-5.8%}	9.057(5) ^{+2.9%} _{-3.0%}	1.36	1.08
$W_L^+ W_T^-$ (DPA)	44.08(1) ^{+5.6%} _{-6.5%}	48.24(4) ^{+1.9%} _{-2.5%}	1.09	1.04
$W_T^+ W_L^-$ (DPA)	50.19(1) ^{+5.5%} _{-6.4%}	54.02(4) ^{+1.9%} _{-2.5%}	1.08	1.03
$W_T^+ W_T^-$ (DPA)	99.61(2) ^{+3.7%} _{-4.6%}	106.20(7) ^{+1.6%} _{-1.9%}	1.07	1.09

Table 3. Fiducial cross-sections (in fb). Same observables as in Table 1.

3.2 Fiducial phase-space region

Relying on the validation of our definition of polarized signals performed in the inclusive setup, we are ready to present results in the fiducial region targeting a realistic analysis of polarized W^+W^- production at the LHC.

The cuts on final-state leptons are expected to generate non-negligible interferences both at the level of total cross-sections and in differential distributions. This renders the analytic expressions in Eq. (3.2) not valid anymore: their application in the presence of realistic lepton cuts (as done in Ref. [17]) gives results that can be far from the actual polarization structure of the process.

In analogy with Table 1, we show in Table 3 singly- and doubly-polarized fiducial cross-sections. At the integrated level, the results feature common aspects with those obtained in the inclusive setup. The contribution of NLO QCD corrections is slightly enhanced by the lepton cuts both for the unpolarized and for the singly-polarized case (+2%). The doubly-polarized cross-sections undergo a +1% increase of the K -factors for those cross-sections involving at least one transverse boson. On the contrary, the K -factor for the LL cross-section is 12% smaller than in the inclusive setup but still much larger than for other polarization combinations. The combination of NLO QCD results with those for the gluon-induced process leads to an enhancement of 1% relative to the inclusive setup for all polarization combinations. The transverse polarization is dominant both in the singly- and in the doubly-polarized case. However, even the LL cross-section promises a reasonable number of events with the luminosity accumulated during Run 2 of the LHC. This gives us confidence that a detailed study of doubly-polarized signals will be performed in this process.

Starting from the results of Table 3, we have evaluated the polarization fractions in the singly-polarized case, as well as the contributions of non-resonant irreducible background and interferences for the fiducial cross-section (see Table 4). Similar to the inclusive setup, the polarization fractions are very stable against QCD radiative corrections, featuring again

	LO	NLO QCD
non-resonant background	0.0302(4) $^{+0.0008}_{-0.0009}$	0.0258(7) $^{+0.0003}_{-0.0002}$
interferences	0.017(1)	0.020(2)
$W_L^+ W_{\text{unpol}}^-$ (DPA)	0.260(1) $^{+0.002}_{-0.003}$	0.268(1) $^{+0.001}_{-0.001}$
$W_T^+ W_{\text{unpol}}^-$ (DPA)	0.723(2) $^{+0.003}_{-0.003}$	0.712(2) $^{+0.001}_{-0.001}$

Table 4. Fractions for a polarized W^+ boson produced in association with an unpolarized W^- boson in the fiducial region. Uncertainties are computed with 7-point scale variations. The polarization fractions are obtained by taking the ratio of polarized total cross-sections over the unpolarized one in the DPA.

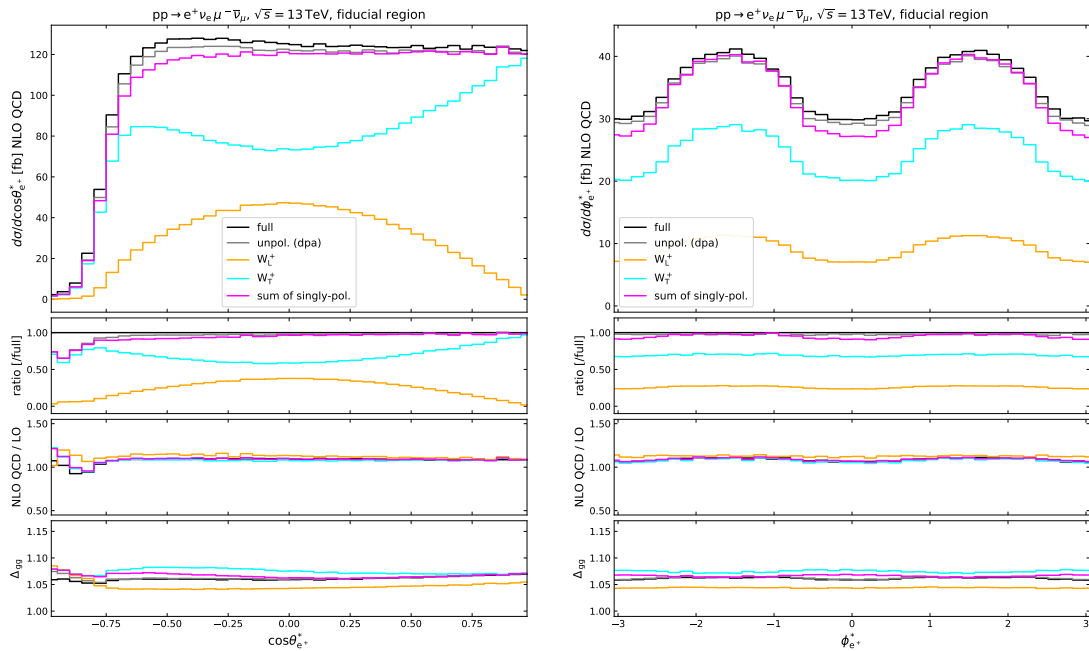
a $\pm 1\%$ modification between LO and NLO QCD and against scale variations. Furthermore, the polarization fractions in the fiducial phase space are similar to those computed in the inclusive setup.

In the fiducial region, the non-resonant background contributions are slightly enhanced, as they account for 2.6% of the full cross-section at NLO QCD, which should be compared with the 1.1% in the absence of selection cuts. The application of cuts on the lepton kinematics (in particular on the transverse momentum of a single lepton) induces non-vanishing interferences among polarization states, which amount to 2% of the full unpolarized result. This contribution is small but non-negligible even at the integrated level. We show below that at the differential level, the interference effects are strongly enhanced in certain phase-space regions.

We now present polarized distributions for some selected kinematic variables. We stress that only a limited number of them represents measurable quantities at the LHC. However, studying non-measurable quantities enables us to find possible similarities with other LHC observables.

We start by showing in Fig. 4 how fiducial cuts modify the angular distributions of leptons in the corresponding W rest frame. We recall that these distributions would be optimal to discriminate among different polarization modes of decayed weak bosons, if they could be reconstructed at the LHC (which is not the case). The effect of lepton cuts is different for the various polarization modes, as can be observed comparing Fig. 4 with Fig. 2. Since the distribution in the transverse momentum of the W boson [Fig. 5(a)] peaks near $p_{T,W} \approx 40 \text{ GeV} \approx M_W/2$, the transverse-momentum cut on single leptons suppresses the production of charged leptons which propagate in the opposite direction of the corresponding decayed boson ($\theta_e^* \approx \pi$). This effect causes the drastic reduction of polarized cross-sections near $\cos \theta_e^* = -1$, while other cuts contribute to the suppression at larger $\cos \theta_e^*$. Thus, the cuts strongly modify the transverse-momentum distribution of the positron, in particular, the component of a left-handed W^+ boson, which would be maximal for $\cos \theta_e^* = -1$ in the absence of cuts. The cuts also destroy the symmetry of the distribution about $\cos \theta_e^* = 0$ for a longitudinal W boson.

An expected consequence of the cuts is the presence of non-vanishing interferences



(a) Cosine of polar angle of e^+ in the W^+ CM frame. (b) Azimuthal angle of e^+ in the W^+ CM frame.

Figure 4. Distributions in the positron angular variables $\cos \theta_e^*$ and ϕ_e^* computed in the W^+ rest frame in the fiducial region. Singly-polarized and unpolarized results are shown. Same subplot structure as in Fig. 2.

among polarization modes, which are mostly evident in the phase-space regions directly affected by the cuts. This is the case for the negative region of the $\cos \theta_e^*$ distribution where they account for 5–7%, as can be extracted by comparing the violet and gray curves in Fig. 4(a). Moreover, the effect of the non-resonant irreducible background is large near $\cos \theta_e^* = -1$, where a sizeable fraction of the doubly-resonant contributions is cut away. For $\cos \theta_e^* > 0$ the interferences are less than 2%, and the DPA is behaving well.

The K -factor is roughly equal for the polarized and unpolarized cases. As already seen at the integrated level, the gluon-induced partonic channel has a different effect on the spin modes of the W^+ boson, enhancing the cross-section for transverse polarization by +7.5% but the longitudinal one by +4%.

The ϕ_e^* distribution shown in Fig. 4(b) features the same $\cos 2\phi_e^*$ modulation as in the inclusive setup (Fig. 3) but with a relatively larger amplitude, which is now present also in the longitudinal component. The agreement between the unpolarized DPA and the full distribution is very good and independent of ϕ_e^* over the whole range, while the interferences are a bit enhanced in the minima of the distribution, where they amount to 8% of the full result. The NLO QCD corrections and the gg-channel contribution are in line with the integrated results.

We now present transverse-momentum variables. We have already investigated missing- p_T distributions in the inclusive setup for polarized W bosons. Because of the bad description of the unpolarized process by the DPA, this variable is not well suited for the extraction

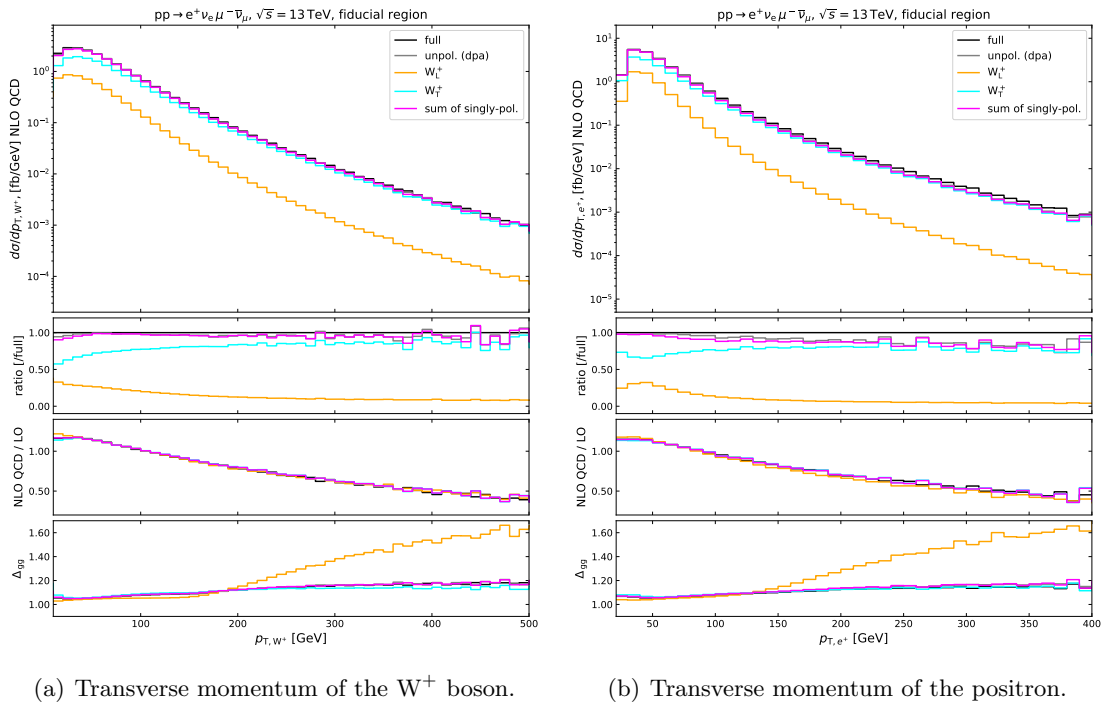


Figure 5. Distributions in the transverse momentum of the W^+ boson and positron in the fiducial region. Singly-polarized and unpolarized results are shown. Same subplot structure as in Fig. 2.

of polarized signals. Therefore, we show no results for this in the fiducial region.

In Fig. 5 we provide the distributions in the transverse momentum of the W^+ boson (not observable) as obtained from Monte Carlo truth and of the positron (observable). Since the positron is part of the decay products of the W^+ boson, we expect that the polarized results for the two variables feature similar behaviour. We consider the configuration in which only the W^+ boson has a definite polarization state. First we estimate the quality of the DPA in the unpolarized case from Fig. 5(a) and Fig. 5(b). The transverse-momentum distribution of the W boson is described very well even at large transverse momentum, while the non-resonant effects become of order 20% in the tails of the positron transverse-momentum distribution, in a similar way (but more moderate in size) as for $p_{T,\text{miss}}$. Up to this difference which has nothing to do with the polarizations, the polarized results are similar for W^+ and e^+ both in the shapes of distributions and in the L/T polarization fractions. The only difference is due to a mild enhancement of the transverse component in the soft spectrum of the positron transverse momentum ($20 \text{ GeV} < p_{T,e^+} < 50 \text{ GeV}$). The interferences are very small for the W^+ transverse momentum, somewhat larger but always below 5% for the positron, which is more directly affected by the lepton cuts. The singly-polarized distributions feature differential K -factors that are almost identical to the unpolarized one both in the W^+ and in the e^+ case. The gg channel gives roughly the same 10% enhancement to the transverse and to the unpolarized distribution. In contrast, the longitudinal component is enhanced by more than 50% for $p_{T,W^+} > 400 \text{ GeV}$ and

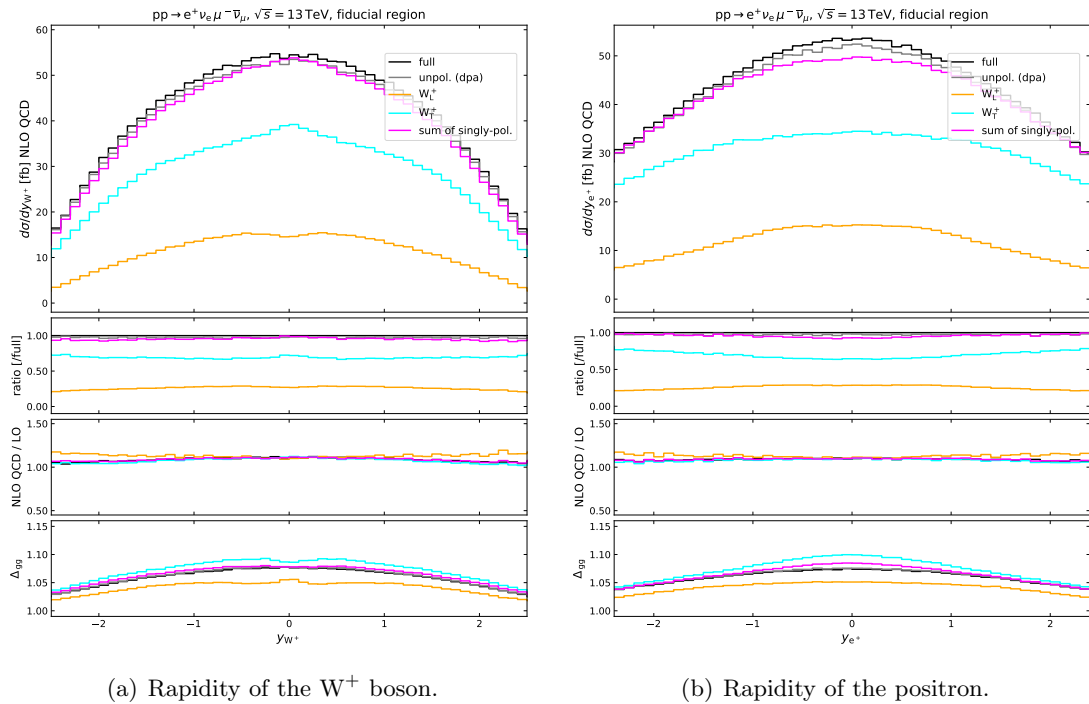


Figure 6. Distributions in the rapidity of the W^+ boson and positron in the fiducial region. Singly-polarized and unpolarized results are shown. Same subplot structure as in Fig. 2.

$p_{T,e^+} > 300$ GeV, which means that in the tails of these distributions the gluonic channel becomes of the same order of magnitude as the quark-induced one for a longitudinal W^+ boson.

Given that off-shell effects are under control and interferences are moderate, the positron transverse momentum represents a good observable for polarized signal separation and a proxy for the W^+ transverse momentum even for a definite polarization state. Similar conclusions can be drawn for the muon and the W^- boson.

Another relevant variable linked to a single W boson is its rapidity. In Figs. 6(a) and 6(b) we show the rapidity distributions for the W^+ boson and the positron, respectively, considering a W^+ boson with definite polarization and an unpolarized W^- boson. It is evident at first glance that the two variables are directly connected. The DPA describes the unpolarized full distribution well, and the interferences are generally small, apart from slightly larger positive effects in the central region of the positron rapidity (at most 8% for $\eta_e^+ = 0$). The K -factors for polarized bosons follow the unpolarized ones, with almost no dependence on the centrality of the W^+ boson or the positron. The gluon-induced process contributes the most in the central region for both variables. The shape of the polarized distributions differs between the transverse and longitudinal polarizations more in the distributions of the W^+ boson. In particular, for $\eta_{W^+} = 0$ the transverse distribution is characterized by a small peak, while the longitudinal one has a local minimum there and peaks near $\eta_{W^+} = \pm 0.4$. This mild effect is reversed in the gluon-induced process. For the

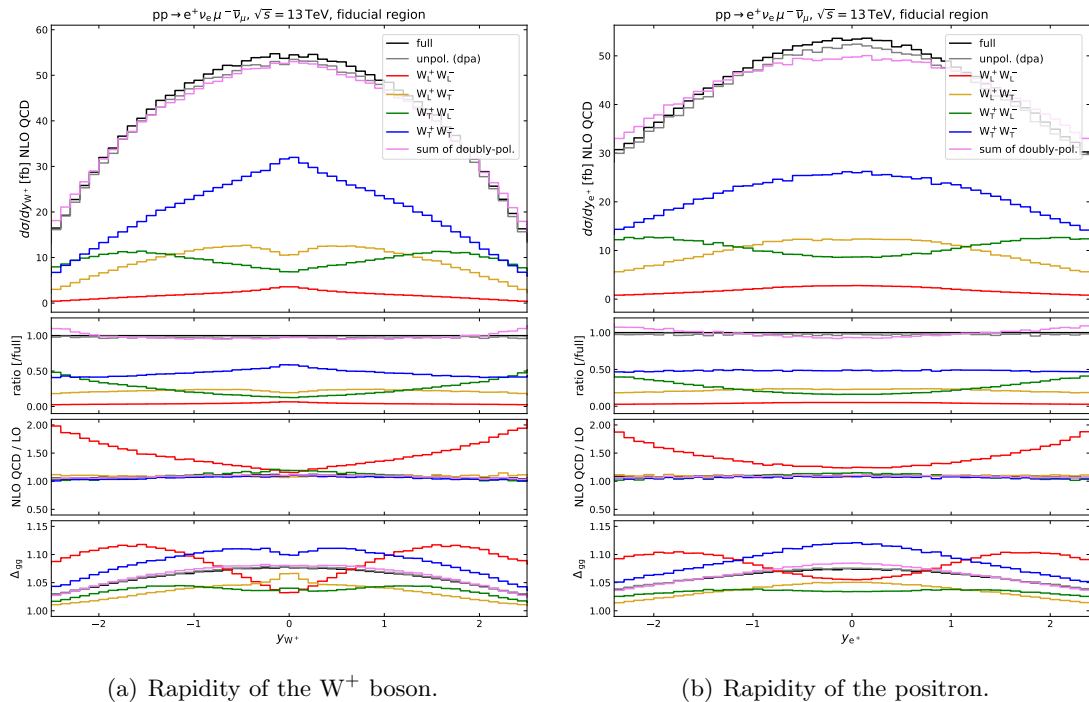


Figure 7. Same as in Fig. 6 but for doubly-polarized distributions.

positron rapidity, the transverse and longitudinal differential cross-sections both feature a maximum in $\eta_e^+ = 0$, and most of the differences show up in the distribution variance, which is slightly smaller in the transverse case. The polarization fractions feature very similar behaviours for the two variables. This gives us further confidence that the positron kinematics can be used as a proxy for the corresponding W^+ -boson kinematics at the level of polarized signals.

In addition to the singly-polarized results in Fig. 6, we present in Fig. 7 the doubly-polarized distributions for the same variables in order to get information about the correlation between the spin states of the two bosons. The interferences are significantly larger than in the singly-polarized configuration at large rapidities of the W^+ boson. Summing over the four combinations of definite polarization states for both W bosons means neglecting the interferences for both bosons. This results in negative interferences of the order of 10% for $|\eta_{W^+}| > 2$. The interferences are smaller in the positron distributions, though slightly larger than in the singly-polarized case. The doubly-polarized K -factors are similar to the unpolarized one, apart from the LL one. In this latter polarization state, the QCD radiative corrections are much larger at forward or backward rapidities, where they reach 100%. However, the LL cross-section is strongly suppressed with respect to other polarization combinations, as already seen for the fiducial cross-section. The gg channel enhances the LL distribution, in particular, in the region $1.5 < |\eta| < 2$ both for the W^+ and for the e^+ . Its contribution to the TT cross-section peaks at $|\eta_{W^+}| \approx 0.5$ and at $\eta_{e^+} = 0$. The mixed combinations receive the smallest enhancement by this partonic channel.

The most interesting aspect of the doubly-polarized distributions concerns their shapes, which give much more information than the singly-polarized ones. As a general statement, the positron rapidity distributions look like a smoothed version of the W^+ rapidity ones. The distribution for a transversely polarized W^+ boson changes drastically depending on whether the W^- boson is longitudinal or transverse. In the former case, the W^+ rapidity distribution peaks at $|\eta_{W^+}| \approx 1.7$ and has a local minimum for $\eta_{W^+} = 0$, while in the latter case, the maximum is at zero rapidity. Similar comments hold for the e^+ rapidity distribution. Note that for $2.0 < |\eta_e^+| < 2.5$ the TL component becomes of the same order of magnitude as the TT one. These correlation effects could be helpful in discriminating experimentally between the boson polarization modes. The other mixed distribution (W^+ longitudinal, W^- transverse) features two symmetric peaks in $|\eta_{W^+}| \approx 0.4$ and a local minimum at $\eta_{W^+} = 0$. However, this does not correspond to an analogous behaviour in the rapidity distribution of the positron, which is almost flat in the region $|\eta_{e^+}| < 0.5$. The LL η_e^+ distribution has a maximum at zero rapidity, which is much less pronounced than the corresponding maximum of the η_{W^+} distribution. Figures 6 and 7 show that extending the investigation to doubly-polarized signals is definitely needed to completely understand the spin structure in di-boson production beyond the extraction of the single-boson angular coefficients.

We present in Fig. 8(a) the distribution in the invariant W^+ mass reconstructed from Monte Carlo truth by summing the positron and electron-neutrino momenta. Though not observable at the LHC, this variable provides interesting information about the DPA description of the full kinematics. The full distribution, which includes all resonant and non-resonant diagrams, is not symmetric about the W pole mass, but favours invariant-mass values larger than M_W . The employed DPA technique projects the kinematics of the amplitude numerator on the mass shell, preserving off-shell kinematics in the (symmetric) Breit–Wigner modulation in W -boson propagators. This renders the invariant-mass distributions more symmetric about the pole mass, as can be seen in Fig. 8(a). The discrepancy between the approximated and full results is in fact positive for $M_{e^+\nu_e} < M_W$ and negative otherwise. It reaches $\pm 50\%$ for $M_{e^+\nu_e} = M_W \mp 20$ GeV. The polarized distributions have more or less the same shape, and their sum reproduces almost perfectly the unpolarized DPA results, in spite of the application of lepton cuts. All these considerations hold with no modification at LO for both the $q\bar{q}$ and the gluon-induced partonic processes as well as at NLO QCD for the quark-induced process.

The invariant mass of the system formed by the two charged leptons is definitely observable at the LHC. The corresponding doubly-polarized distributions are shown in Fig. 8(b). The DPA reproduces the full result reasonably well, in particular in the region $M_{e^+\mu^-} < 400$ GeV where the discrepancies between the two unpolarized predictions are below 10%. In the same region, the polarization interferences are of order of 10%, negative for $M_{e^+\mu^-} < 100$ GeV and positive between 100 and 300 GeV. In the tails of the distributions, the non-resonant effects dominate the discrepancy with respect to the full result (15%), while the interferences are negligible. The same effects can be found even in the inclusive setup, as well as in the study of singly-polarized distributions. It seems likely to be related to the strong correlation between the bosons in W -pair production, as well as to

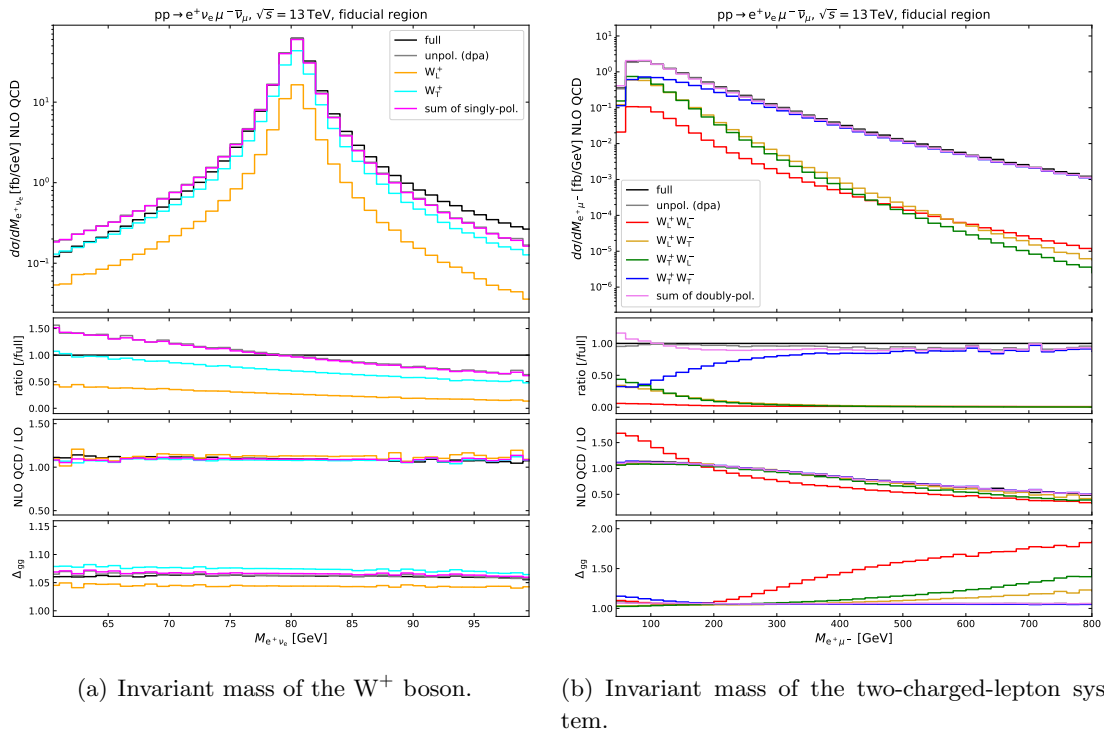


Figure 8. Distributions in the invariant masses of the W^+ boson (from Monte Carlo truth) and of the two charged leptons in the fiducial region. Singly-polarized results are shown in Fig. 8(a), doubly-polarized ones in Fig. 8(b). Same subplot structure as in Fig. 2.

the binning of the distributions which introduces implicit cuts on the variable itself (as for other leptonic kinematic variables). For $M_{e^+\mu^-} > 500$ GeV the LL component is larger than the mixed ones. However, all of the three combinations involving at least one longitudinal boson are strongly suppressed in the high-mass region (two orders of magnitude smaller than the doubly-transverse one). In the soft region of the spectrum (where interferences are sizeable) the TL/LT contributions are even larger than the TT one. Given the limited experimental statistics, the soft part of the spectrum is the only one which is accessible and worth investigating. Furthermore, given the Higgs-background cut $M_{e^+\mu^-} > 55$ GeV imposed on this variable, it would be interesting to study the effect of varying such a cut on the polarized distributions. The K -factors are below one for invariant masses larger than 200 GeV, and the LL one decreases faster than the others. On the contrary, in the soft region, K -factors are above one and the LL one is much higher than the others. The gg channel enhances the configurations with at least one longitudinal boson for $M_{e^+\mu^-} > 200$ GeV. In the tails of the distributions this contribution becomes of the same order of magnitude as the quark-induced one for the LL signal.

In Fig. 9 we present doubly-polarized distributions for two different angular variables between the two charged leptons. In the azimuthal separation [Fig. 9(a)], which we already investigated in the inclusive setup in Fig. 3(b), the distributions in the presence of lepton cuts feature a peak near $\Delta\phi_{e^+\mu^-} \approx 2.6$ (it is π in the inclusive setup). The interference

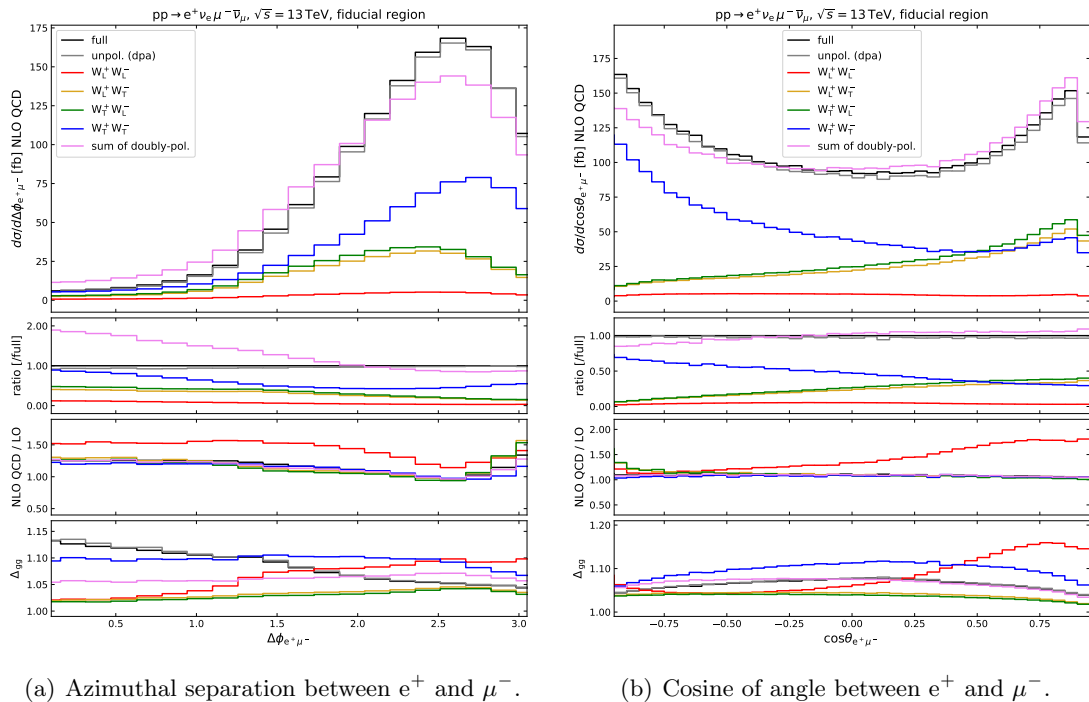


Figure 9. Distributions in the azimuthal separation and in the cosine of the angle between the two charged leptons in the fiducial region. Doubly-polarized results are shown. Same subplot structure as in Fig. 2.

effects discussed in Sect. 3.1 are strongly enhanced and reach almost 100% for $\Delta\phi_{e^+\mu^-}$ close to zero. Apart from the modification of the shapes, the lepton cuts do not change the conclusions that we have drawn in the inclusive setup. A possible improvement in the description of this variable could only be given by a cut. Since the Higgs signal is enhanced for $\Delta\phi_{e^+\mu^-} < 1.8$ [65], selecting the complement of the spectrum helps extracting more precisely the di-boson signal. Note that imposing $\Delta\phi_{e^+\mu^-} > 1.8$ would also mean excluding the region which is dominated by large negative interferences.

In Fig. 9(b) the distribution in $\cos\theta_{e^+\mu^-}$ (computed in the laboratory frame) is presented. At the unpolarized level, the two leptons tend to be produced in a collinear configuration, if lepton cuts are absent. This is in agreement with the fact that the positron is preferably produced in the opposite direction of the W^+ boson, while the muon is produced mostly in the same direction of the W^- boson, as can be also deduced from $\cos\theta_\ell^*$ distributions. However, the application of selection cuts on the leptons impedes the collinear configuration ($\cos\theta_{e^+\mu^-} = 1$) and the resulting situation is the following: the TT contribution has its maximum at $\cos\theta_{e^+\mu^-} = -1$, while the mixed contributions peak at values slightly smaller than $\cos\theta_{e^+\mu^-} = 1$. Note that the TL and LT contributions have the same shape but differ in the overall normalization according to the total cross-sections shown in Table 3. The LL distribution vanishes for collinear leptons and is almost flat in the rest of the spectrum up to a very mild tendency to prefer negative values of $\cos\theta_{e^+\mu^-}$. The DPA reproduces very well the full computation in this distribution. The interferences are

moderate and feature a change of sign at $\cos\theta_{e^+\mu^-} = 0$. For positive values of the variable they are negative and account at most for 10%, while for negative values they are positive and amount to 15–20% in the back-to-back configuration. The QCD corrections enhance the mixed and LL contributions by roughly 20% for $\cos\theta_{e^+\mu^-} \approx -1$. Furthermore, the LL distribution benefits from the radiative corrections in the positive side of the spectrum, where the corrections are again of order 50%. It receives a similar enhancement of up to 15% also from the combination with the gluon-induced channel. This partonic process enhances the TT signal by more than 10% in the central part of the distribution. The good DPA description of the unpolarized cross-section, the presence of interferences that are sizeable but can be taken into account in the SM, and the clear differences in the shapes of polarized distributions make this angular observable a good candidate for the discrimination of polarized signals at the LHC.

4 Conclusion

In this paper we have studied W-pair production at the LHC with one or both bosons in definite polarization states. We have included NLO QCD corrections to the leading $q\bar{q}$ partonic process as well as the loop-induced gluon-initiated contribution at LO.

The polarized signals are defined at the amplitude level and rely on the double-pole approximation. The doubly-resonant contributions are separated in a gauge-invariant way at LO and at NLO QCD, including the (integrated and unintegrated) subtraction counterterms and the real corrections. Amplitudes for polarized vector bosons are defined based on the gauge-invariant doubly-resonant contributions in the double-pole approximation. This strategy is radically different from other methods that have been used in the literature to define polarized cross-sections for unstable particles. In particular, this technique allows one to define polarized cross-sections while retaining some off-shell effects and all spin correlations. We have evaluated the quality of thus-defined polarized signals both in terms of the missing off-shell effects and in terms of the interferences among polarization states. The results are not limited to the polarization of a single boson but target a more complete description of the spin structure of the process by means of the doubly-polarized signals, which give access to the correlation between the polarization modes of the two bosons.

We have presented total and differential cross-sections both in an inclusive setup and in a fiducial region that mimics the one of the most recent ATLAS measurement in W^+W^- production. The inclusive setup serves as a validation framework: the comparison with results extracted from unpolarized distributions via projection on polarized angular distributions gives very good agreement for both singly- and doubly-polarized signals. As a by-product, we have found that already in the inclusive setup some observables are subject to large interferences and non-resonant background effects, and thus not well suited to extract the weak-boson polarizations. In the fiducial region, we have investigated the effect of a realistic set of cuts on distributions for polarized and unpolarized bosons with the aim to identify the observables that are particularly sensitive to the polarization of decayed bosons, and more in general to understand how the polarization selection modifies the distributions with respect to the unpolarized case.

The polarization fractions are very stable against scale variations, and the related theoretical error is usually at the sub-percent level both at LO and NLO QCD. The NLO-QCD K -factors for singly-polarized processes are very close to the ones of the full computation. The same holds for doubly-polarized cross-sections that feature at least one transverse W boson. The distributions for purely longitudinal W bosons receive very large K -factors despite the application of a jet veto.

From the combination of the quark- and gluon-induced contributions, we verified that the spin structure of the initial state influences the final-state polarization modes considerably owing to the limited number of final-state particles.

This represents a first realistic study of vector-boson polarizations in W^+W^- hadronic production, which will hopefully help addressing future experimental analyses that target the extraction of polarized signals from LHC data.

Acknowledgements

We are grateful to Jean-Nicolas Lang for supporting RECOLA and to Timo Schmidt and Mathieu Pellen for maintaining MOCANLO. GP thanks Alessandro Ballestrero and Ezio Maina for useful discussions. The authors acknowledge financial support by the German Federal Ministry for Education and Research (BMBF) under contract no. 05H18WWCA1.

References

- [1] **CMS** Collaboration, S. Chatrchyan et al., *Measurement of the Polarization of W Bosons with Large Transverse Momenta in W +Jets Events at the LHC*, *Phys. Rev. Lett.* **107** (2011) 021802, [[arXiv:1104.3829](#)].
- [2] **ATLAS** Collaboration, G. Aad et al., *Measurement of the polarisation of W bosons produced with large transverse momentum in pp collisions at $\sqrt{s} = 7$ TeV with the ATLAS experiment*, *Eur. Phys. J.* **C72** (2012) 2001, [[arXiv:1203.2165](#)].
- [3] **ATLAS** Collaboration, G. Aad et al., *Measurement of the angular coefficients in Z -boson events using electron and muon pairs from data taken at $\sqrt{s} = 8$ TeV with the ATLAS detector*, *JHEP* **08** (2016) 159, [[arXiv:1606.00689](#)].
- [4] **CMS** Collaboration, V. Khachatryan et al., *Angular coefficients of Z bosons produced in pp collisions at $\sqrt{s} = 8$ TeV and decaying to $\mu^+\mu^-$ as a function of transverse momentum and rapidity*, *Phys. Lett.* **B750** (2015) 154–175, [[arXiv:1504.03512](#)].
- [5] **ATLAS** Collaboration, M. Aaboud et al., *Measurement of the W boson polarisation in $t\bar{t}$ events from pp collisions at $\sqrt{s} = 8$ TeV in the lepton+jets channel with ATLAS*, [[arXiv:1612.02577](#)].
- [6] **CMS** Collaboration, V. Khachatryan et al., *Measurement of the W boson helicity fractions in the decays of top quark pairs to lepton + jets final states produced in pp collisions at $\sqrt{s} = 8$ TeV*, *Phys. Lett.* **B762** (2016) 512–534, [[arXiv:1605.09047](#)].
- [7] **CMS, ATLAS** Collaboration, G. Aad et al., *Combination of the W boson polarization measurements in top quark decays using ATLAS and CMS data at $\sqrt{s} = 8$ TeV*, [[arXiv:2005.03799](#)].

- [8] **ATLAS** Collaboration, M. Aaboud et al., *Measurement of $W^\pm Z$ production cross sections and gauge boson polarisation in pp collisions at $\sqrt{s} = 13$ TeV with the ATLAS detector*, *Eur. Phys. J. C* **79** (2019) 535, [[arXiv:1902.05759](#)].
- [9] **CMS** Collaboration, *Vector Boson Scattering prospective studies in the ZZ fully leptonic decay channel for the High-Luminosity and High-Energy LHC upgrades*, Tech. Rep. CMS-PAS-FTR-18-014, CERN, Geneva, 12, 2018.
- [10] P. Azzi et al., *Report from Working Group 1: Standard Model Physics at the HL-LHC and HE-LHC*, in *Report on the Physics at the HL-LHC, and Perspectives for the HE-LHC* (A. Dainese, et al., eds.), vol. 7, pp. 1–220. CERN, 12, 2019. [[arXiv:1902.04070](#)].
- [11] Z. Bern et al., *Left-Handed W Bosons at the LHC*, *Phys. Rev.* **D84** (2011) 034008, [[arXiv:1103.5445](#)].
- [12] W. J. Stirling and E. Vryonidou, *Electroweak gauge boson polarisation at the LHC*, *JHEP* **07** (2012) 124, [[arXiv:1204.6427](#)].
- [13] A. Belyaev and D. Ross, *What Does the CMS Measurement of W-polarization Tell Us about the Underlying Theory of the Coupling of W-Bosons to Matter?*, *JHEP* **08** (2013) 120, [[arXiv:1303.3297](#)].
- [14] A. Ballestrero, E. Maina, and G. Pelliccioli, *W boson polarization in vector boson scattering at the LHC*, *JHEP* **03** (2018) 170, [[arXiv:1710.09339](#)].
- [15] A. Ballestrero, E. Maina, and G. Pelliccioli, *Polarized vector boson scattering in the fully leptonic WZ and ZZ channels at the LHC*, *JHEP* **09** (2019) 087, [[arXiv:1907.04722](#)].
- [16] A. Ballestrero, A. Belhouari, G. Bevilacqua, V. Kashkan, and E. Maina, *PHANTOM: A Monte Carlo event generator for six parton final states at high energy colliders*, *Comput.Phys.Commun.* **180** (2009) 401–417, [[arXiv:0801.3359](#)].
- [17] J. Baglio and N. Le Duc, *Fiducial polarization observables in hadronic WZ production: A next-to-leading order QCD+EW study*, *JHEP* **04** (2019) 065, [[arXiv:1810.11034](#)].
- [18] J. Baglio and L. D. Ninh, *Polarization observables in WZ production at the 13 TeV LHC: Inclusive case*, *Commun. Phys.* **30** (2020) 35–47, [[arXiv:1910.13746](#)].
- [19] D. Buarque Franzosi, O. Mattelaer, R. Ruiz, and S. Shil, *Automated predictions from polarized matrix elements*, *JHEP* **04** (2020) 082, [[arXiv:1912.01725](#)].
- [20] P. Artoisenet, R. Frederix, O. Mattelaer, and R. Rietkerk, *Automatic spin-entangled decays of heavy resonances in Monte Carlo simulations*, *JHEP* **03** (2013) 015, [[arXiv:1212.3460](#)].
- [21] Q.-H. Cao, B. Yan, C.-P. Yuan, and Y. Zhang, *Probing $Zt\bar{t}$ couplings using Z boson polarization in ZZ production at hadron colliders*, [[arXiv:2004.02031](#)].
- [22] A. Aeppli, F. Cuypers, and G. J. van Oldenborgh, *$O(\Gamma)$ corrections to W pair production in e^+e^- and $\gamma\gamma$ collisions*, *Phys. Lett.* **B314** (1993) 413–420, [[hep-ph/9303236](#)].
- [23] A. Aeppli, G. J. van Oldenborgh, and D. Wyler, *Unstable particles in one loop calculations*, *Nucl. Phys.* **B428** (1994) 126–146, [[hep-ph/9312212](#)].
- [24] W. Beenakker, F. A. Berends, and A. P. Chapovsky, *Radiative corrections to pair production of unstable particles: results for $e^+e^- \rightarrow 4$ fermions*, *Nucl. Phys.* **B548** (1999) 3–59, [[hep-ph/9811481](#)].
- [25] A. Denner, S. Dittmaier, M. Roth, and D. Wackerroth, *Electroweak radiative corrections to*

- $e^+e^- \rightarrow WW \rightarrow 4$ fermions in double-pole approximation: The RACOONWW approach, *Nucl. Phys.* **B587** (2000) 67–117, [[hep-ph/0006307](#)].
- [26] M. Billoni et al., *Next-to-leading order electroweak corrections to $pp \rightarrow W^+W^- \rightarrow 4$ leptons at the LHC in double-pole approximation*, *JHEP* **12** (2013) 043, [[arXiv:1310.1564](#)].
- [27] B. Biedermann, et al., *Next-to-leading-order electroweak corrections to $pp \rightarrow W^+W^- \rightarrow 4$ leptons at the LHC*, *JHEP* **06** (2016) 065, [[arXiv:1605.03419](#)].
- [28] A. Bierweiler, T. Kasprzik, J. H. Kühn, and S. Uccirati, *Electroweak corrections to W -boson pair production at the LHC*, *JHEP* **11** (2012) 093, [[arXiv:1208.3147](#)].
- [29] F. Caola, K. Melnikov, R. Röntsch, and L. Tancredi, *QCD corrections to W^+W^- production through gluon fusion*, *Phys. Lett. B* **754** (2016) 275–280, [[arXiv:1511.08617](#)].
- [30] M. Grazzini, S. Kallweit, S. Pozzorini, D. Rathlev, and M. Wiesemann, *W^+W^- production at the LHC: fiducial cross sections and distributions in NNLO QCD*, *JHEP* **08** (2016) 140, [[arXiv:1605.02716](#)].
- [31] M. Grazzini, S. Kallweit, J. M. Lindert, S. Pozzorini, and M. Wiesemann, *NNLO QCD + NLO EW with Matrix+OpenLoops: precise predictions for vector-boson pair production*, *JHEP* **02** (2020) 087, [[arXiv:1912.00068](#)].
- [32] E. Re, M. Wiesemann, and G. Zanderighi, *NNLOPS accurate predictions for W^+W^- production*, *JHEP* **12** (2018) 121, [[arXiv:1805.09857](#)].
- [33] S. Kallweit, E. Re, L. Rottoli, and M. Wiesemann, *Accurate single- and double-differential resummation of colour-singlet processes with MATRIX+RadISH: W^+W^- production at the LHC*, [[arXiv:2004.07720](#)].
- [34] S. Bräuer, A. Denner, M. Pellen, M. Schönherr, and S. Schumann, *Fixed-order and merged parton-shower predictions for WW and WWj production at the LHC including NLO QCD and EW corrections*, [[arXiv:2005.12128](#)].
- [35] M. Chiesa, C. Oleari, and E. Re, *NLO QCD+NLO EW corrections to diboson production matched to parton shower*, [[arXiv:2005.12146](#)].
- [36] J. Kühn, F. Metzler, A. Penin, and S. Uccirati, *Next-to-Next-to-Leading Electroweak Logarithms for W -Pair Production at LHC*, *JHEP* **06** (2011) 143, [[arXiv:1101.2563](#)].
- [37] J. Baglio, S. Dawson, and I. M. Lewis, *An NLO QCD effective field theory analysis of W^+W^- production at the LHC including fermionic operators*, *Phys. Rev. D* **96** (2017) 073003, [[arXiv:1708.03332](#)].
- [38] **OPAL** Collaboration, G. Abbiendi et al., *W^+W^- production and triple gauge boson couplings at LEP energies up to 183 GeV*, *Eur. Phys. J. C* **8** (1999) 191, [[hep-ex/9811028](#)].
- [39] **ATLAS** Collaboration, M. Aaboud et al., *Measurement of the W^+W^- production cross section in pp collisions at a centre-of-mass energy of $\sqrt{s} = 13$ TeV with the ATLAS experiment*, *Phys. Lett. B* **773** (2017) 354–374, [[arXiv:1702.04519](#)].
- [40] **ATLAS** Collaboration, M. Aaboud et al., *Measurement of fiducial and differential W^+W^- production cross-sections at $\sqrt{s} = 13$ TeV with the ATLAS detector*, *Eur. Phys. J. C* **79** (2019) 884, [[arXiv:1905.04242](#)].
- [41] R. G. Stuart, *Gauge invariance, analyticity and physical observables at the Z^0 resonance*, *Phys. Lett. B* **262** (1991) 113–119.

- [42] A. Denner and S. Dittmaier, *Electroweak Radiative Corrections for Collider Physics*, *Phys. Rept.* **864** (2020) 1–163, [[arXiv:1912.06823](#)].
- [43] S. Catani and M. Seymour, *A general algorithm for calculating jet cross-sections in NLO QCD*, *Nucl. Phys. B* **485** (1997) 291–419, [[hep-ph/9605323](#)]. [Erratum: *Nucl. Phys. B* 510 (1998) 503–504].
- [44] W. Beenakker, A. P. Chapovsky, and F. A. Berends, *Non-factorizable corrections to W pair production: Methods and analytic results*, *Nucl. Phys.* **B508** (1997) 17–63, [[hep-ph/9707326](#)].
- [45] A. Denner, S. Dittmaier, and M. Roth, *Non-factorizable photonic corrections to $e^+e^- \rightarrow WW \rightarrow$ four fermions*, *Nucl. Phys.* **B519** (1998) 39–84, [[hep-ph/9710521](#)].
- [46] S. Actis, A. Denner, L. Hofer, A. Scharf, and S. Uccirati, *Recursive generation of one-loop amplitudes in the Standard Model*, *JHEP* **04** (2013) 037, [[arXiv:1211.6316](#)].
- [47] S. Actis, et al., *RECOLA: REcursive Computation of One-Loop Amplitudes*, *Comput. Phys. Commun.* **214** (2017) 140–173, [[arXiv:1605.01090](#)].
- [48] A. Denner and R. Feger, *NLO QCD corrections to off-shell top-antitop production with leptonic decays in association with a Higgs boson at the LHC*, *JHEP* **11** (2015) 209, [[arXiv:1506.07448](#)].
- [49] A. Denner and M. Pellen, *NLO electroweak corrections to off-shell top-antitop production with leptonic decays at the LHC*, *JHEP* **08** (2016) 155, [[arXiv:1607.05571](#)].
- [50] A. Denner, J.-N. Lang, M. Pellen, and S. Uccirati, *Higgs production in association with off-shell top-antitop pairs at NLO EW and QCD at the LHC*, *JHEP* **02** (2017) 053, [[arXiv:1612.07138](#)].
- [51] A. Denner and M. Pellen, *Off-shell production of top-antitop pairs in the lepton+jets channel at NLO QCD*, *JHEP* **02** (2018) 013, [[arXiv:1711.10359](#)].
- [52] B. Biedermann, A. Denner, and M. Pellen, *Complete NLO corrections to W^+W^+ scattering and its irreducible background at the LHC*, *JHEP* **10** (2017) 124, [[arXiv:1708.00268](#)].
- [53] B. Biedermann, A. Denner, and M. Pellen, *Large electroweak corrections to vector-boson scattering at the Large Hadron Collider*, *Phys. Rev. Lett.* **118** (2017) 261801, [[arXiv:1611.02951](#)].
- [54] A. Denner, S. Dittmaier, P. Maierhöfer, M. Pellen, and C. Schwan, *QCD and electroweak corrections to WZ scattering at the LHC*, *JHEP* **06** (2019) 067, [[arXiv:1904.00882](#)].
- [55] **Particle Data Group** Collaboration, M. Tanabashi et al., *Review of Particle Physics*, *Phys. Rev. D* **98** (2018) 030001.
- [56] D. Bardin, A. Leike, T. Riemann, and M. Sachwitz, *Energy-dependent width effects in e^+e^- annihilation near the Z-boson pole*, *Phys. Lett. B* **206** (1988) 539–542.
- [57] A. Buckley, et al., *LHAPDF6: parton density access in the LHC precision era*, *Eur. Phys. J. C* **75** (2015) 132, [[arXiv:1412.7420](#)].
- [58] **NNPDF** Collaboration, R. D. Ball et al., *Parton distributions from high-precision collider data*, *Eur. Phys. J. C* **77** (2017) 663, [[arXiv:1706.00428](#)].
- [59] A. Denner, S. Dittmaier, M. Roth, and L. Wieders, *Electroweak corrections to charged-current $e^+e^- \rightarrow$ 4 fermion processes: Technical details and further results*, *Nucl. Phys. B* **724** (2005) 247–294, [[hep-ph/0505042](#)]. [Erratum: *Nucl. Phys. B* 854 (2012) 504].

- [60] A. Denner and S. Dittmaier, *The complex-mass scheme for perturbative calculations with unstable particles*, *Nucl. Phys. Proc. Suppl.* **160** (2006) 22–26, [[hep-ph/0605312](#)].
- [61] T. Binoth, M. Ciccolini, N. Kauer, and M. Krämer, *Gluon-induced W -boson pair production at the LHC*, *JHEP* **12** (2006) 046, [[hep-ph/0611170](#)].
- [62] P. F. Monni and G. Zanderighi, *On the excess in the inclusive $W^+W^- \rightarrow l^+l^-\nu\bar{\nu}$ cross section*, *JHEP* **05** (2015) 013, [[arXiv:1410.4745](#)].
- [63] T. Becher, R. Frederix, M. Neubert, and L. Rothen, *Automated NNLL + NLO resummation for jet-veto cross sections*, *Eur. Phys. J. C* **75** (2015) 154, [[arXiv:1412.8408](#)].
- [64] E. Maina, *Vector boson polarizations in the decay of the Standard Model Higgs*, [arXiv:2007.12080](#).
- [65] **ATLAS** Collaboration, G. Aad et al., *Observation and measurement of Higgs boson decays to WW^* with the ATLAS detector*, *Phys. Rev. D* **92** (2015) 012006, [[arXiv:1412.2641](#)].